

# GMRT study of Wolf Rayet galaxies

Shweta Srivastava<sup>(1)</sup>, N. G. Kantharia<sup>(2)</sup>

(1) Astronomy & Astrophysics Deptt., Physical Research Laboratory, Ahmedabad - 380 009, India

(2) National Centre for Radio Astrophysics, TIFR, Pune - 411007, India

## Abstract:

We report multi-frequency radio continuum observations of few Wolf Rayet galaxies Mrk 8, Mrk 1089, Mrk 33, Mrk 1236 and NGC 3049 using the Giant Meter-wave Radio Telescope (GMRT). It is remarked that these galaxies have not so far been detected and studied at much lower frequencies. Our investigations reveal that many of these galaxies are detected at frequencies  $< 1$  GHz. We estimate synchrotron spectral index after separating the thermal free-free emission and obtain  $\alpha_{nt} = 1$  to  $-0.4$ . The radio morphology of the galaxies resembles the UV emission seen by GALEX with and extent similar to the NIR emission from 2MASS.

## 1. Introduction:

The Wolf-Rayet (WR) galaxies are characterized as a subtype of star-burst galaxies where a large portion of stars of the star-burst is of WR stars. The WR galaxies exhibit, in their integrated spectra, most commonly a broad He II 4686 feature originating in the stellar winds of their stars. Detection and analysis of WR stellar populations in young star-burst is a powerful tool to reveal the properties of the star-forming events. The most recent survey for WR features using the SDSS Data Release 6 (Adelman et al. 2008) was performed by Brichmann et al. 2008 who detected 570 galaxies with significant WR features and a further 1115 potential candidates. Later studies revealed the presence of other WR signatures notably the broad emission lines of NIII 4640 and/ CIII 4650 as well as CIV 5808. WR galaxies are one of the best laboratories to study star-burst properties since these objects harbor the most massive stars known, O stars and their descendants WR stars, which allow to probe the upper part of the IMF and the youngest stellar populations. Due to their strong emission lines they can be identified in nearby galaxies. Some of these galaxies have been studied at radio wavelengths (Klein et al. 1991; Beck et al. 2000; Deeg et al. 1993; Ramya et al. 2011). We are studying the properties of a sample of WR galaxies using the GMRT combining with the higher frequency data from literature (Srivastava et al. 2014). In this paper, we present the radio continuum observations at 150, 240, 325 and 610 MHz tracing the combined distribution of thermal and non-thermal radiation for the five WRs. This is the first time that many of these galaxies have been detected at frequencies  $< 1$  GHz. Combined with the higher frequency observations from Very Large Array (VLA) data archive the radio spectra can be modeled. The distance to these galaxies is less than 100 Mpc. Table 1 lists the general properties of these galaxies.

**Mrk 008:** This galaxy has a striking and unusual optical and H $\alpha$  morphology of clumps in an elongated ring (Bottinelli et al. 1975) which has led it to be classified as a recent merger product.

**Mrk 1089:** Mrk 1089, which has traditionally been classified as a double-nucleus Markarian galaxy (MB). This galaxy is a member of Hickson Compact Group 31, the several galaxies of which are merging (Mendes et al. 1994; Moles et al. 1994). NGC 1741 hosts a very strong star-formation event, which is very probably a consequence of the merging of two spiral galaxies.

**Mrk 33:** This galaxy is the brightest known BCG ( $m_B = 13.4$  and  $M_B = -18.4$  from Loose et al. 1986) in our sample. This galaxy has a blue central star-burst ( $B-V = 0.36$ ), which sits inside a regular, extended elliptical envelope. The radio emission measured at lower resolution by Moellenhoff et al. (1992) is not centered on the optical source but on a dust lane offset from the optical center. Similar structures are seen in NGC 5253 and He 2-10 and may be the signature of an accretion event.

**Mrk 1236:** This is a satellite of the spiral galaxy NGC 3023 (Kunth et al. 1986) that is optically bright and is called a star-burst and a low metallicity BCD. A broad He II 4686 emission line in this galaxy was seen by Kunth et al. 1986 and confirmed by Vacca et al. 1992).

**NGC 3049:** This galaxy also known as Mrk 710 in the Markarian & Lipovetskii (1976) catalog is classified as SBbp in Markarian (1979). This is a barred spiral galaxy, in the Virgo cluster, and also classified as a nuclear star-burst (Balzano et al. 1983), a W-R galaxy (Conti 1991), and a H II galaxy (Tterlevich et al. 1991). This low-mass galaxy has a small bulge and a thin bar of constant surface brightness surrounded by an inner ring (Contini et al. 1997).

This paper is structured as follows. Section 2 gives an account of the observations and data reduction. Section 3 gives a note on individual galaxies. Section 4 is a detailed discussion on our results and section 5 summarizes the study.

## **2. Observation and Data Reduction:**

All the galaxies were observed using the GMRT (Swarup, 1991) in the radio continuum at 150, 240 and 610 MHz. The 240 and 610 MHz observations were simultaneous in the dual band mode. All the observations were done in the non-polar mode of observing known as the Indian polar mode. The duration of the observation was about 5 hrs for each galaxy at each of the frequencies. Since the galaxies Mrk 1236 and NGC 3049 are closely located in the sky plane, they were observed in the same observing run with common calibration scans. Both the target source scans alternated between the two galaxies resulting in better uv - coverage for both the galaxies. Observational Parameters and details of the beam size, position angle along with rms noise of each galaxy at each particular frequency are presented respectively in Table 2. The data analysis has been done following standard procedures in AIPS. After initial round of flagging a single channel data of the amplitude calibrator was set to its known value.

Once the gain calibration became satisfactory, i.e. the closure errors were less than one percent, the bandpass gain table were applied to the data. This calibration was applied to all the data and then several channels were averaged to form a continuum database. Care was taken to avoid bandpass smearing. Flagging of bad data was effected at all stages of data analysis. On the average we lost ~16 % of data at 150 MHz and 240 MHz and ~ 9 % of data at 610 MHz. Images were then generated using multiple facets to avoid wide-field effects. Finally, self calibration was applied to the data before generating the final images. Moreover we made maps using different robust weighting which resulted in different beam sizes and signal-to-noise ratios. We also made images with different uv ranges to study features at a range of different angular scales. The final images were corrected for primary beam attenuation before undertaking flux measurements. Moreover, the 240 MHz data of the galaxies Mrk 1236 and NGC 3049 were corrupted due to which extensive flagging of data had to be done and the final image quality was suspect. We, hence, do not use our 240 MHz data.

## **3. Results & Discussion**

Flux densities of the galaxies at the different GMRT frequencies along-with at other frequencies obtained from literature are listed in Table 3. In all the presented images to follow, north is up and east is towards the left. All the galaxies have been detected at the respective observed wave bands except Mrk 33, which was not detected at 150 MHz. The images obtained are presented in Figures 1 to 8. Figures 1, 2 and 3 show the radio continuum map of Mrk 8, Mrk 1089 and Mrk 33 respectively. Figures 7 and 8 show the radio images of Mrk 1236 and NGC 3049 at 610 MHz respectively with gray images overlaid on them. The rms noise in the final 610 MHz maps is in the range 0.2 - 0.4  $\mu$ Jy whereas it is about 2.5 mJy for the 240 MHz images. The rms noise in the 150 MHz continuum maps range from 3.0 to 5.0 mJy. We present in the sequel a discussion on individual galaxies.

### **3.1 Individual Sources:**

**Mrk 8:** This galaxy, which has a complex optical morphology, is detected at all the three bands i.e. 610, 240 and 150 MHz. Figure 1 shows the radio contour images of Mrk 8 at these frequencies superposed on the radio gray scale image. At 610 MHz although the galaxy is not resolved but the radio peaks are seen to be centered on the eastern part of the galaxy. Additionally, the emission is extended towards the north along a narrow ridge of emission. A radio tail-like emission is also detected at 610 MHz in south east direction with estimated flux density  $27.4 \pm 4.1$  mJy. On the other hand, radio emission at 244 and 150 MHz is noticed to be mostly associated from the center of the galaxy. A weak radio emission in the south east direction at 150 MHz partly matches with the emission at 610 MHz. We use NVSS map of Mrk 8 for the spectral index study. As NVSS detects emission from the entire disk of the galaxy, we use the NVSS map, which has an angular resolution of 45 arc-sec, along-with our 150 MHz made with robust 0 weighting. We generate a spectral index map of the radio emission between 150 and 1420 MHz after smoothing the 150 MHz image with the NVSS resolution. The spectral index across the galaxy is found to vary from -1.2 to -0.4.

**Mrk 1089:** This galaxy, as pointed out earlier, is the member labeled as C of the group HCG 31. Emission from this galaxy as well as from other members A, B, E and G are detected at 610 MHz (see Figure 2). Strong radio emission is seen at the center of the group which is mainly from Mrk 1089. The flux density at 610 MHz, after excluding the flux density of others members of the group, comes out to be  $36.1 \pm 5.4$  mJy. However, the other group members were in the field of radio observations but they are not detected. The radio emission at 240 and 150 MHz is detected only from Mrk 1089 and not from other members of the group. We estimated its flux density of  $58.6 \pm 8.8$  and  $74.6 \pm 11.2$  mJy at 240 and 150 MHz respectively. The integrated spectral index between 610 and 150 MHz is  $\sim -0.5$ . We use the NVSS map of Mrk 1089, which has an angular resolution of 45 arc-sec, along-with our 150 MHz made with Robust=0 weighting after smoothing to the NVSS resolution to generate a spectral index map of the radio emission between 150 and 1420 MHz. The image pixels below 3 sigma in the input images were clipped before calculation of the spectral index. The spectral index across the galaxy is found to vary from -0.9 to -0.4.

**Mrk 33:** The continuum maps of this galaxy at 244 and 610 MHz are shown in the Figure 3. . We do not detect the galaxy at 150 MHz within 3 sigma limit of 15 mJy. Figure 3(a) shows the radio map at 610 MHz with an integrated flux density of about  $30.9 \pm 4.6$  mJy. At both the observed frequencies no individual compact sources can be distinguished/resolved. The radio continuum emission arises in the central parts of the galaxy and, which extends to the northwest. A little amount of radio emission is also extended to the north from the center. The continuum emission encompasses the entire optical galaxy. The radio spectral index between 610 and 244 MHz comes out to be  $\sim -1.0$  which shows that most of the emission at lower frequency is non-thermal.

**Mrk 1236:** The radio emission from this galaxy at 610 MHz with robust weighting 5 are presented in Figure 7. It has revealed to possess the same basic structure as of a very strong central source embedded in a weak envelope. Two radio peaks are detected in which one is at the center of the galaxy. An arm like structure is seen to the northwest, but as the rms of this image is high, this could also be an imaging error. We were not able to image this galaxy at lower frequencies i.e. at 244 and 150 MHz. Due to the various artifacts coming in the image, the radio map was not beneficial and hence the flux density at these frequencies could not be estimated. Higher sensitivity radio data are required so as to confirm the existence and the nature of the radio feature.

**NGC 3049 :** The radio image of NGC 3049 with robust weighting 5 at 610 MHz is presented in Figure 8. The radio emission is entirely coming from the galaxy core which seems to be a strong star-burst region. In addition to the center, radio emission is traced out from an envelope in the form of a bar extending towards north-east. But no radio emission is seen in the south eastern arm. The halo emission is seen around the bar structure and most of the emission is extended towards north. In the region of halo emission two radio peaks are visible but the more pronounced emission is from the central bulge.

### 3.2 Morphology and emissions at various wavebands

The radio contours of the sample galaxies at 610 MHz are shown in Figures 5 to 8 superposed on the GALEX NUV and 2MASS NIR images. Each of the galaxy reveals an interesting morphology. The UV emission means the galaxy to be undergoing vigorous star formation whereas, the IR emission tells about the old stellar population. Radio continuum appears to be more extended than the NIR emission for all the sample galaxies.

Mrk 8, as one can see in its NUV image (Figure 5), does not get resolved into the separate galaxies. Interestingly, two of the distinctly appearing galaxy constituents of Mrk 8 prominent in radio images do not get resolved in its NUV image. The distinctly appearing galaxy is clearly visible in the optical picture of the galaxy (see Figure 5c). The radio emission is entirely covering the NUV disk. The 2MASS image (Figure 5b) also resolves the two interlocking galaxies to some extent. It is not extended as in its radio image revealing that the older stellar population is lying at the center of this galaxy. We have also superposed the radio image on the HST image (Figure 5c) of this galaxy, which clearly correlates with the extension of the radio emission. The eastern arm is more extended than the western arm.

Similarly for Mrk 1089 we can see that the optical (Figure 6a), radio and NUV (Figure 6b) emission fairly correlates with one another. The morphological feature of radio and UV is quite similar but the radio emission is more pronounced indicating a fairly recent star formation episode in these regions. Most of the H $\alpha$  emission is visible from the members C and G of the group HCG 31. No NIR (Figure 6c) emission is detected along the bridge or from the star forming regions. The IR emission is only visible from the members C and G. A very faint NIR emission is seen from the arm like extension in the southwest, which is much more pronounced in the radio, optical and UV. There are no infra-red observations available that can separate A and B, but the CO observations of Yun (1997) show that the molecular gas, which usually correlates with the dust, is centered on B. The HI map of the group by Williams et al. (1991) shows that all the galaxies are embedded in the same gas cloud and the maximum of H I column density coincides with the optical galaxies; indicating they are gas-rich.

In the galaxy Mrk 33, the emission in radio and NUV fairly matches whereas, IR emission is only concentrated to the center. In Figure 4, we have overlaid the radio continuum contours at 610 MHz, made from Robust=5 weighting, on the GALEX NUV map and on the NIR image from 2MASS, respectively. Summers et al. (2001) find an extended, complex, shell-like morphology in the X-ray emission of Mrk 33 coincident with the bright star-forming regions at the center of the galaxy. They also concluded that the physical extent of H $\alpha$  and X-ray emission is very similar. HI observation of Mrk 33 reveals that the extent of emission roughly coincides with the optical feature and the HI halo is extended than the optical feature. Bravo-alfaro et al. (2004) suggested that Mrk 33 has acquired substantial amount of gas as a result of interaction or recent merger. The HI bears little resemblance to the radio continuum at 610 MHz. HI mass of Mrk 33 is  $2.3 \pm 0.2 \times 10^8 M_{\odot} \text{ yr}^{-1}$  (Bravo-alfaro et al. 2004).

We have also compared the radio emission of Mrk 1236 with NUV and 2MASS which are shown in Figures 7 and 8 respectively. The compact radio emission in the east direction matches well with the NUV emission. Both the bands show similar kind of extent in their emission. The UV emission appears to be of irregular morphology with the star formation having been triggered at various locations along a arm like structure extending towards north east, which quite resemble with the radio emission. The NIR image of the galaxy shown in Figure 6c displays the emission only from the center of the galaxy. No extended emission is seen in the NIR image other than the center. Radio continuum appears to be more extended than the NIR emission. Thus one can say that the old stellar population is only distributed in a the compact region and superposed on this spherical distribution of old stars is the light from the younger population of stars which are detected in the NUV band of the GALEX.

In NGC 3049 there are sites of very young (5 Myr) starburst evidenced by the presence of WR stars (Contini et al. 1995). The north-east extension along the bar of the galaxy is much stronger in the radio than in the NUV (Figure 7b). NUV emission coming from the bar as well a halo is also seen entirely covering the bridge bar emission. Similarly, in radio emission also we see a extended emission around the bar in the northeast. The enhanced emission in both bands i.e. NUV and radio is coming from the central bulge. Its IUE spectrum suggests a young stellar population dominating the central emission (Mas-Hasse et al. 1999). Molecular gas has also been reported to be detected at the center of this galaxy (Contini et al. 1997). FUV image of Gonzalez et al. (2002) also show extended emission along the bar. NGC 3049 is very bright in the FIR ( $L_{\text{IR}} = 9 \times 10^{42} \text{ ergsec}^{-1}$ ; (Heckman et al. 1998) and at UV wavelengths (Kinney et al. 1993). The optical image of this galaxy shows extended recent star formation along the bar (Mazzarella et al. 1993; Contini 1997). The two bright optical knots embedded in the bar cannot be distinguished in the radio image. The 2MASS NIR image of this galaxy is totally concentrated along the bar shown in Figure 8c, whereas radio emission is much more extended in comparison to the NIR. At least six much weaker clusters are detected in the center of NGC 3049 (Gonzalez et al. 2002) and most of the emission is dominated by a very bright central cluster. Dust in the diffuse ISM dominates the IR power in Mrk 33 and NGC 3049 (Contini, 1995).

### 3.3 Radio continuum spectra:

In this subsection, we discuss the global spectrum of the galaxies after combining our three-frequency radio data with the existing radio data available in the literature. We plot the spectra, employing the data presented in Table 3, in Figure 9 on log-log scale. These plots are only showed for the galaxies for which till date sufficient data is available. Since the higher frequency data i.e.  $\nu > 1.4 \text{ GHz}$  is available but of very high resolution and not sensitive to our angular scale. Thus, for some of the galaxies we cannot comment on their behavior at these frequencies.

The radio luminosity for an individual star forming galaxy has been suggested to be directly proportional to the SFR; which can be traced to recently formed massive ( $M \leq 8 M_{\odot}$ ) stars (Condon, 1992). The continuum emission at 1.4 GHz from extremely massive stars is about 10 % due to free-free emission (thermal emission) and the rest 90 % is almost synchrotron radiation coming from relativistic electrons accelerated in the remnants of core-collapse supernovae. Accordingly, studying the continuum emission one may discriminate the older and supernova regions from younger and mostly thermal areas (Deeg et al. 1993, Beck et al. 2000; Cannon et al. 2004). The radio continuum observations at different wavelengths have been used to quantify the non-thermal and thermal contributions. With a view to trace thermal emission from these galaxies we have used flux density of  $\text{H}\alpha$  emission as  $\text{H}\alpha$  and thermal free-free emissions originate from recombination of the same ionized gas. In order to have an estimate of the thermal emission at 1.4 GHz we have used the equation provided by Dopita et al. (2002).

$$F_{1.4\text{GHz thermal}} = 1.21 \times 10^{12} F_{\text{H}\alpha}$$

Here,  $F_{\text{H}\alpha}$  is taken in units of  $\text{erg cm}^{-2} \text{ s}^{-1}$  and the result comes in mJy. The  $\text{H}\alpha$  flux values are obtained from the literature. A comparison of  $F_{1.4\text{GHz thermal}}$  and  $F_{1.4\text{GHz}}$  allows the estimation of the non-thermal flux. One can also estimate the non-thermal to thermal ratio, R after separating the thermal and non-thermal component (Dopita et al. 2002). On an average its value for star-burst galaxies is given via  $\log R = 1.3 \pm 0.4$ .

We have modeled the observed integrated radio continuum emission under the assumption that the observed emission: (1) is non-thermal synchrotron emission and (2) is a combination of thermal free-free and non-thermal synchrotron emission along the line of sight. We have estimated the thermal free-free emission at radio frequencies by extrapolating the thermal free-free emission from  $\text{H}\alpha$  assuming that both arise in ionized star forming regions, which is a realistic assumption, and is optically thin and follow a  $\nu^{-0.1}$ . The green curve in Figure 9 shows the thermal emission estimated in this way. The optically thin free-free emission was then removed from the total flux density at all the frequencies and the remnant flux was considered to be due to synchrotron emission (blue curve

in Figure 9). As discussed, the non-thermal flux at 1.4 GHz is estimated using H $\alpha$  flux and using the relation (Equation 1). The radio spectral index of Mrk 8 is found to be  $-0.4 \pm 0.1$ . Heidmann et al. (1987) has found the value to be about  $-0.7$ . The strong star formation episode observed in Mrk 8 is due to the interaction of two (or three) disk galaxies (Esteban et al. 1999). The HI mass for this galaxy determined by Bottinelli et al. (1975) is  $1 \times 10^{10} M_{\odot}$ . We have also estimated the parameter ( $q$ ) (Condon, 1991) which is a measure of the star-burst versus AGN nature of the radio emission. Normal galaxies which show the FIR-radio (1.4 GHz) correlation have a value of  $q = 2.35 \pm 0.2$  (Condon, 1992; Yun et al. 2001), while we observed  $q = 2.24$  for Mrk 8 which is within the observed scatter for the correlation.

The non-thermal spectral index for Mrk 1089 comes out to be  $-0.59 \pm 0.04$ . We have determined the SFR for Mrk 1089 using its 1.4 GHz radio luminosity to be  $2.0 M_{\odot} \text{ yr}^{-1}$ . Compared to this the SFR obtained by Lopez-Sanchez (2008) is  $\sim 2.9 M_{\odot} \text{ yr}^{-1}$ , whereas the other obtained by using FIR fluxes is equal to  $3.3 M_{\odot} \text{ yr}^{-1}$ . We estimate  $q = 2.38$  which agrees with the FIR-radio correlation within errors. A similar value ( $q = 2.39$ ) has also been reported by Lopez-Sanchez (2010b).

Radio observations of Mrk 33 show it to have a steep spectrum of  $\alpha = -0.9 \pm 0.2$  which is consistent with the value of  $\alpha = -0.82 \pm 0.12$  (Klein, 1984); suggesting the presence of non-thermal sources such as of supernova remnants. More recent results by Beck et al. (2000) show the presence of both thermal and non-thermal emission with the former coming mainly from the outer regions of the galaxy and not from point sources, while the latter comes mainly

from the inner regions. Recent H $\alpha$  imaging of Mrk 33 (Mendez et al., 2000) has revealed the presence of at least three star-forming knots in the center of the galaxy. Mrk 33 does not appear to have any obvious companions. However, there is a very red galaxian object, B-R = 1.7 (USNO A 2.0 catalog), lying at a projected distance  $\sim 30$  kpc (Monet, 1998). Moellenhoff et al. (1992) detected a radio source with no obvious optical counterpart at  $\sim 3.2$  kpc north of Mrk 33. As there is no kinematic data available for either of these objects, it is impossible to say whether they have any associations with Mrk 33. Bravo – Alfaro (2004) estimated the rate of formation of massive stars using the relations of Condon, 1992. They obtained  $\text{SFR}_{1.4 \text{ GHz}} = 0.28 M_{\odot} \text{ year}^{-1}$ ,  $\text{SFR}_{\text{H}\alpha} = 0.39 M_{\odot} \text{ year}^{-1}$  and  $\text{SFR}_{\text{FIR}} = 0.33 M_{\odot} \text{ year}^{-1}$ .

For Mrk 1236, we have data points for only two frequencies i.e. 610 and 1400 MHz. We estimated the radio spectral index at these frequencies which comes out to be  $\sim -0.1$ . The 20 to 6 cm spectrum of Mrk 1236 falls like that of a normal spiral galaxy (Beck et al. 2000). The  $q$  value could not be estimated due to the lack of IRAS FIR fluxes in the literature.

The radio emission of NGC 3049 is non-thermal showing a steep spectrum of  $\alpha = -0.5 \pm 0.1$

between 610 and 1400 MHz. Beck et al. 2000 found the range of  $\alpha = -1.0$  to  $-0.6$  in the frequency range between 5 to 15 GHz. This is typical value of a classic star-burst spiral galaxy. Further, the emission is found to be entirely from the galaxy core. Due to lack of H $\alpha$  fluxes data in the literature, the modeling of the spectra for Mrk 1236 and NGC 3049 could not be done.

#### 4. Conclusions:

We have presented the preliminary analysis of five WR galaxies observed with GMRT at 610, 240 and 150 MHz. We have compared the radio continuum emission with the NUV and 2MASS bands and for most of the galaxy we find similar correlations with these bands. We further note that the emission in NUV is much more extended than the emission in IR suggesting that all the sample galaxies are undergoing vigorous star formation. We find that a power law spectrum nicely fits the data between 1400 & 150 MHz. The integrated radio spectra of the galaxies are modeled over the frequency range. Separation of the non-thermal from the thermal emission employing the H $\alpha$  flux results in  $\alpha_{\text{nt}}$  ranging from  $-1.0$  to  $-0.4$ ; confirming the general result that the non-thermal emission dominates at the lower frequencies. At higher frequencies ( $> 1.4$  GHz) WR galaxies have a flatter spectrum compared to spiral star-burst galaxies. We have interpreted the results in context of the thermal and non-thermal components of the radio emission that should arise in the star-burst

regions. Thermal fluxes relate to the ultraviolet luminosity of ionizing stars and non-thermal fluxes to the number of supernovae. It is inferred that the star formation of galaxies studied has recently been triggered and that the environment in which the galaxy is evolving has played an important role. Most of the galaxies in the sample are interacting and said to be chemically evolved gas-rich objects. This gives strength to the concept that galaxy interactions could be an important channel to produce the strong star formation activity leading to the WR galaxies. Our low frequency observations, therefore, gives important inputs on the non-thermal spectral index. For future, we would like to have a better image of Mrk 33, Mrk 1236 and NGC 3049 at 150 MHz. We have also observed Mrk 1236 and NGC 3049 at 330 MHz, which we will like to include further for our spectral index study. Besides, high-resolution infra-red observations and deeper radio observations of these WR galaxies would be interesting.

Table1:General properties of the galaxies

| <b>Parameter</b>               | <b>Mrk 8</b> | <b>Mrk 1089</b> | <b>Mrk 33</b> | <b>Mrk 1236</b> | <b>NGC 3049</b> |
|--------------------------------|--------------|-----------------|---------------|-----------------|-----------------|
| Other names                    | IC 2184      | Mrk 1089        | UGC 5720      | VV 620          | Mrk 710         |
|                                | UGC 3852     | H31 C           | HARO 2        | PGC 028275      | UGC 05325       |
| Optical size                   | 0.8 x 0.4    | 0.6 x 0.2       | 1.18 x 0.8    | 1.0 x 0.52      | 2.13 x 1.07     |
| Helio rd. Vel.                 | 3604         | 4019            | 1430          | 1890            | 1455            |
| Object type                    | G Group      | G               | G             | PofG            | G               |
| Classification                 | Irr          | SB(s)m pec      | H II Im pec   | HII             | SB(rs)ab        |
| Distance                       | 50.2         | 55.5            | 22.1          | 30.8            | 24.6            |
| $M_B$                          | 14.0         | 14.4            | 13.5          | 16.3            | 13.5            |
| $L_{FIR}$ ( $\times 10^{43}$ ) | 3.75         | 7.2             | 1.4           | --              | 0.74            |
| $12+\log[O/H]$                 | 8.51         | 8.04            | 8.40          | 8.06            | 9.03            |
| $f_{60\mu}$                    | 2.46         | 3.92            | 4.73          | –               | 2.7             |
| $f_{100\mu}$                   | 3.96         | 5.84            | 5.25          | --              | 4.3             |

Note: Distances are taken from NED, using a Hubble constant of  $73 \text{ km sec}^{-1} \text{ Mpc}^{-1}$ ; FIR data is obtained from IRAS faint source catalog (source: NED); units of optical size in arcmin, Helio radial velocity in  $\text{km s}^{-1}$ , distance in Mpc,  $L_{FIR}$  in  $\text{erg sec}^{-1}$  and FIR fluxes in Jy

Table 2: Observational Parameters

|                                 | <b>150 MHz</b> | <b>244 MHz</b> | <b>610 MHz</b> |
|---------------------------------|----------------|----------------|----------------|
| Receiver Bandwidth <sup>a</sup> | 8              | 16             | 32             |
| No. of Antenna <sup>b</sup>     | 27             | 29             | 28             |
| Primary Calibrator <sup>c</sup> | 3C147(67.85)   | 3C48(48.0)     | 3C48(29.42)    |
|                                 | 3C286(31.01)   | 3C147(59.14)   | 3C147(38.12)   |
| Telescope time <sup>d</sup>     | 5              | 4.5            | 4.5            |
|                                 |                |                |                |

Note: a in MHz; b Maximum number of antenna operational during the observation; c The values in the parenthesis are the flux densities of the calibrators set by SETJY task ; Using (1999.2) VLA or Reynolds (1934-638) coefficients; d for each galaxy in hours

Table 3: Integrated Radio Flux densities

| <b>Frequency</b> | <b>Mrk 8</b> | <b>Mrk 1089</b> | <b>Mrk 33</b> | <b>Mrk 1236</b> | <b>NGC 3049</b> | <b>References</b> |
|------------------|--------------|-----------------|---------------|-----------------|-----------------|-------------------|
| 150              | 54.9(8.2)    | 74.6(11.2)      | \$<\$15.0     |                 |                 | 1                 |
| 244              | 36.4(5.5)    | 58.6(8.8)       | 57.3(8.6)     |                 |                 | 1                 |
| 610              | 27.4(4.1)    | 36.1(5.4)       | 30.9(4.6)     | 17.2(2.6)       | 11.6(1.7)       | 1                 |
| 1400             | 17.2(0.4)    | 29.6(0.4)       | 12.1(0.4)     | 15.4(1.3)       | 7.2(1.2)        | 5                 |
| 1400             | 12.6         | 22(3)           | 24.6          |                 |                 | 2,3,4             |
| 1490             |              | 31.7(1.6)       |               |                 |                 | 6                 |
| 4890             |              | 6.9(0.6)        |               |                 |                 | 6                 |
| 5000             | 8.2          |                 |               |                 |                 | 2                 |
| 8460             |              | 5.8(0.2)        |               |                 |                 | 6                 |

Note: Numbers in parentheses are the fractional uncertainties in the fluxes, for GMRT fluxes 15 % of error has been taken, units of flux density in mJy and freq. In MHz.

1. This paper; 2. Heeschen et al. (1982); 3. Bravo – Alfaro (2004); 4. Verdes et al. (2005) 5. flux values from NVSS maps; 6. Lopez – Sanchez (2004)

Table 4: Final Summary of Results

| <b>Galaxy</b> | <b>q</b> | <b><math>\alpha_{nth}</math></b> |
|---------------|----------|----------------------------------|
| Mrk 8         | 2.2      | $- 0.4 \pm 0.1$                  |
| Mrk 1089      | 2.4      | $- 0.59 \pm 0.04$                |
| Mrk 33        | 2.6      | $- 0.9 \pm 0.2$                  |
| Mrk 1236      | --       | $\sim - 0.1$                     |
| NGC 3049      | 2.9      | $- 1.1 \pm - 0.2$                |

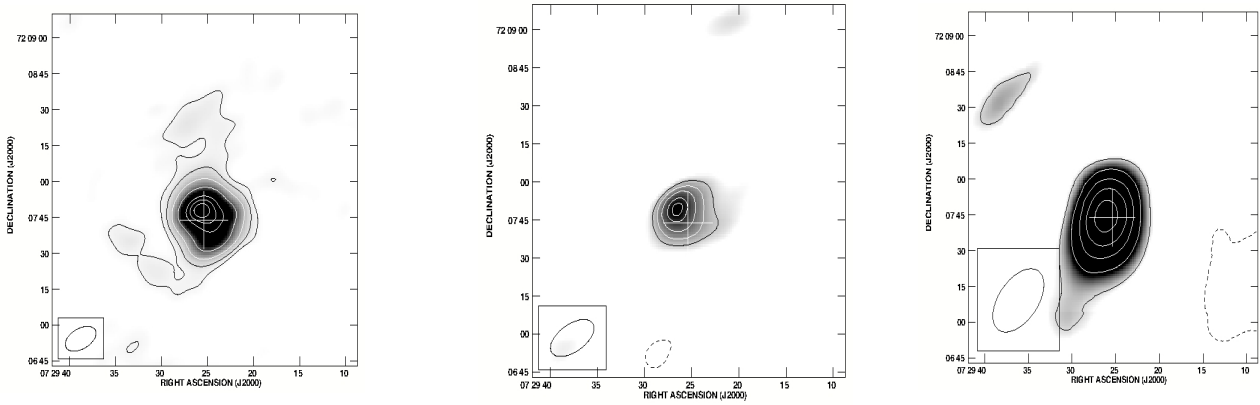


Figure 1. Radio images of Mrk 8 at (a) 610 MHz, beam size =  $16.37 \times 8.76 \text{ arcsec}^2$ , p.a. =  $-66.44^\circ$ , contour levels are  $125 \times (-3, 3, 6, 12, 24, 48, 60) \mu\text{Jy/beam}$ ; (b) 244 MHz, beam size =  $23.15 \times 11.32 \text{ arcsec}^2$ , p.a. =  $-63.03^\circ$ , contour levels are  $2.2 \times (-3, 3, 4, 5, 6, 6.5) \text{ mJy/beam}$ , (c) 150 MHz, beam size =  $33.62 \times 19.69 \text{ arcsec}^2$ , p.a. =  $-46.16^\circ$ , contour levels are  $3.0 \times (-3, 3, 5, 7, 9, 11) \text{ mJy/beam}$

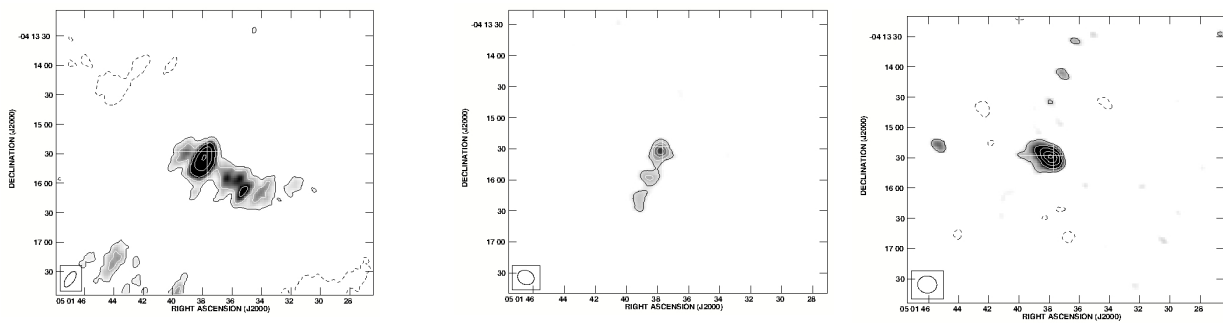


Figure 2. Radio images of (a) 610 MHz, robust weighting 5, beam size =  $18.44 \times 8.15 \text{ arcsec}^2$ , p.a. =  $-34.85^\circ$ , contours levels are  $0.3 \times (-3, 3, 6, 12, 24, 48, 96, 192) \text{ mJy/beam}$ ; (b) 244 MHz, robust weighting 0, beam size =  $16.43 \times 13.51 \text{ arcsec}^2$ , p.a. =  $66.51^\circ$ , contours level are  $2.6 \times (-3, 3, 4, 5, 6) \text{ mJy/beam}$ ; (c) 150 MHz, robust weighting 0, beam size =  $19.17 \times 16.83 \text{ arcsec}^2$ , p.a. =  $84.79^\circ$ , contours levels are  $4 \times (-3, 3, 5, 7, 9, 11) \text{ mJy/beam}$

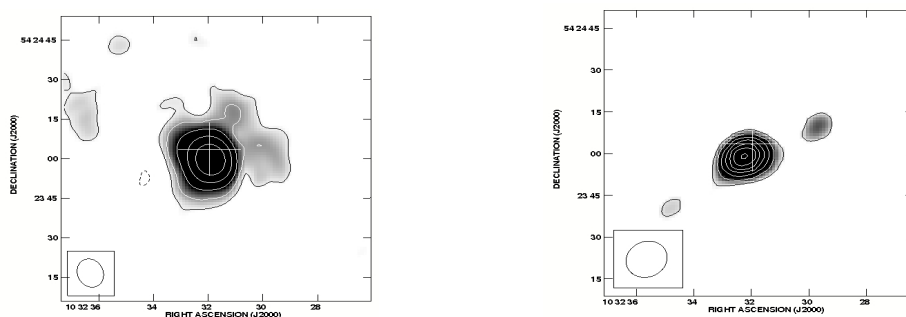


Figure 3. Radio images of Mrk 33 at (a) 610 MHz, robust weighting 5, beam size =  $10.88 \times 8.30 \text{ arcsec}^2$ , p.a. =  $14.77^\circ$ , contours levels are  $0.18 \times (-3, 3, 6, 12, 24, 48) \text{ mJy/beam}$ , (b) 244 MHz, robust weighting 0, beam size =  $13.45 \times 12.02 \text{ arcsec}^2$ , p.a. =  $-33.04^\circ$ , contours levels are  $3.5 \times (-6, 6, 8, 10, 12, 14, 16, 18, 20, 22) \text{ mJy/beam}$

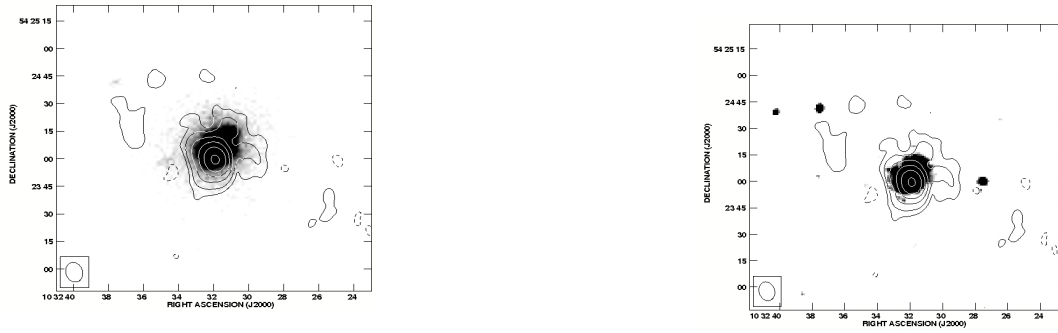


Figure 4. The radio contours of Mrk 33 overlaid on (a) NUV Image (b) 2MASS Image

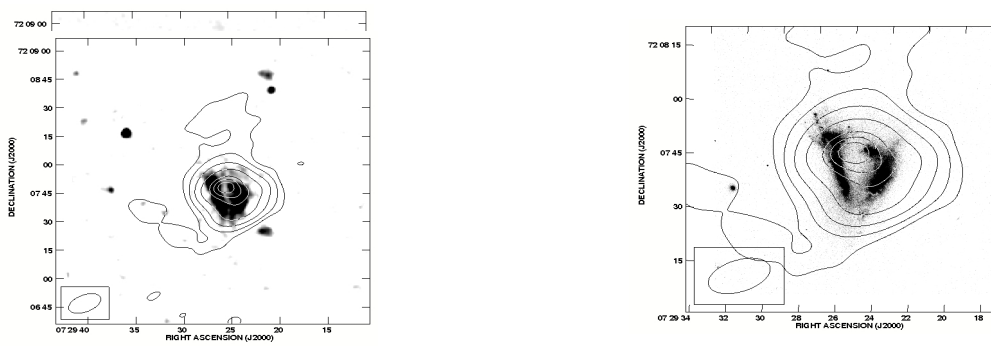


Figure 5. The radio contours of Mrk 8 overlaid on (a) GALEX NUV Image, (b) 2MASS Image, (c) HST Image

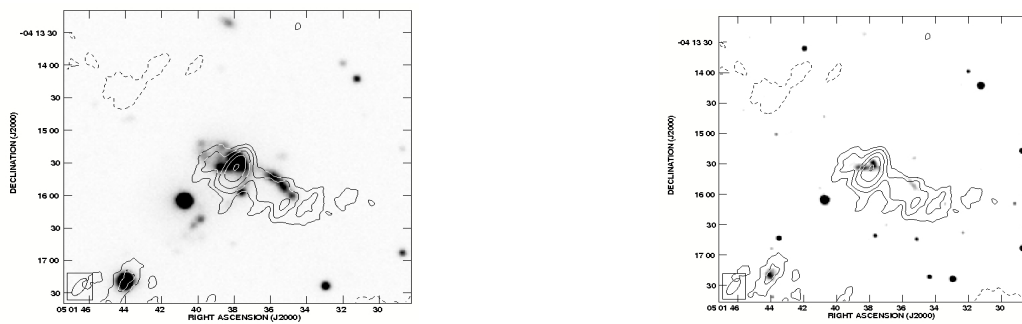


Figure 6. The radio contours of Mrk 1089 overlaid on (a) NUV Image (b) 2MASS Image

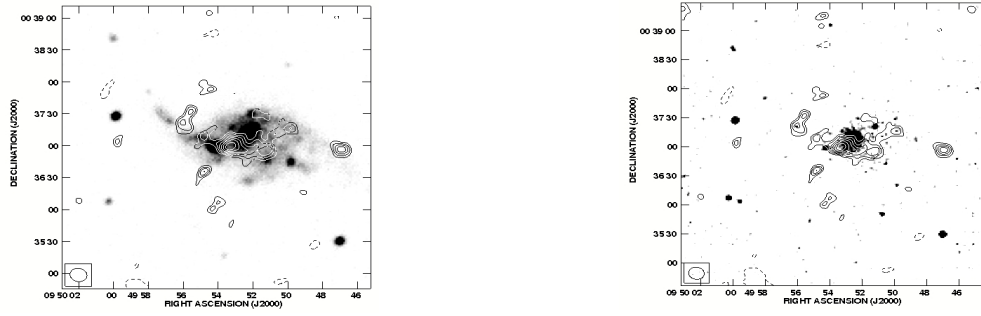


Figure 7. Radio contour of Mrk 1236 overlaid on (a) NUV image, is made by robust weighting 5 and by taking maximum uv cut-off of  $20 \text{ k}\lambda$ , beam size =  $14.71 \times 12.45 \text{ arcsec}^2$ , p.a. =  $76.82^\circ$ , contour levels are  $0.45 \times (-3, 3, 4, 5, 6, 7, 8) \text{ mJy/beam}$ , (c) 2MASS Image

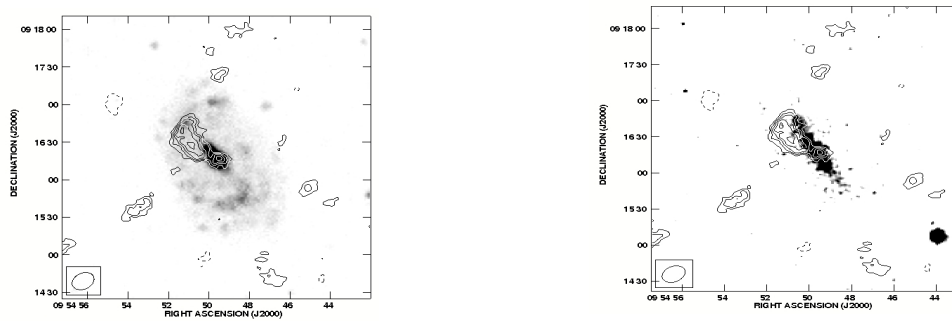


Figure 8. Radio contour of NGC 3049 overlaid on (a) NUV Image, image is made with robust weighting 5, beam size =  $17.03 \times 12.62 \text{ arcsec}^2$ , p.a. =  $-60.50^\circ$ , contour levels are  $0.52 \times (-3, 3, 4, 5, 6, 7, 8) \text{ mJy/beam}$ , (b) 2MASS Image

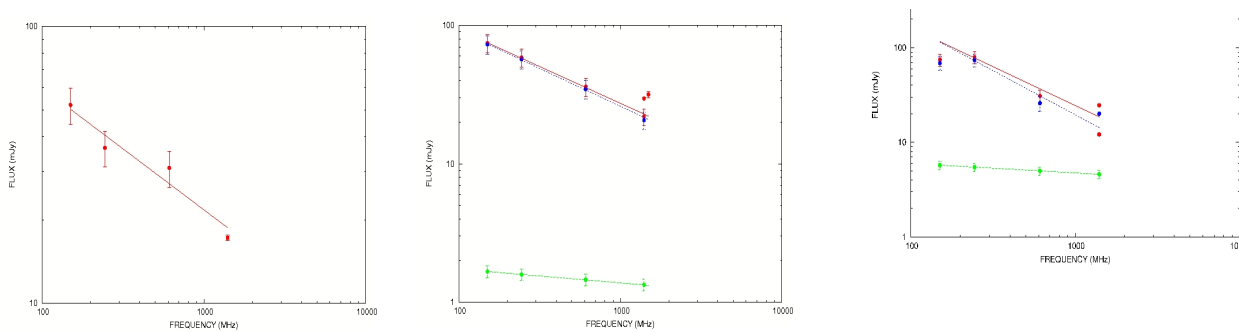


Figure 9. The global radio spectrum of (a) Mrk 8,  $\alpha = -0.63 \pm 0.04$ ; (b) Mrk 1089,  $\alpha_{nt} = -0.59 \pm 0.04$ ; (c) Mrk 33,  $\alpha_{nt} = -1.0 \pm 0.1$ ; the red line represents the total, blue the non-thermal, and green line the thermal components in (b) and (c)